IJSCS

Photo-Induced Creep of Network Polymers

Kevin N. Long, Martin L. Dunn, Timothy F. Scott, H. Jerry Qi[*]

Department of Mechanical Engineering, University of Colorado at Boulder, Boulder, CO 80309

Abstract

We investigate the photo-induced creep behavior of a network polymer that can relax stress upon irradiation at particular wavelengths (Scott et al., 2006; Scott et al., 2005). The underlying mechanism is a photochemical-mediated structural rearrangement of the polymer network through polymer chain cleavage and reformation which results in macroscopic stress relaxation. Previous work on this material focused on photo-induced stress relaxation experiments where the overall deformation of the material is fixed. In that case, evolution of the network structure occurs in a single configuration of the body. In this paper, we investigate simultaneous light-stimulated material evolution and deformation under a creep setup. In contrast to stress relaxation, under photo-induced creep, evolution of the network occurs in different configurations as network relaxation is necessarily accompanied by further deformation of the body. Hence, photo-induced creep involves additional complexity because the newly reformed networks have different stress-free configurations and states of deformation. To model the light-stimulated activity, we decompose the cross-linked network into three parallel networks: an initial, a reformed, and a newly formed network. These three networks are distinguished by their volume fractions, stress-free configurations, and states of deformation. Together, the combined mechanical behavior of all three networks describes the mechanical response of the material. The model is used to predict photo-induced creep behavior under different applied nominal stresses and light intensities. Generally, the model performs well in predicting the overall creep behaviors as well as capturing the trends produced by changing the light intensity and applied nominal stress.

Keywords: Light-activated polymers; Shape-memory polymers; Constitutive modeling; Soft active materials.

1. Introduction

Network polymers which exhibit environmentally activated mechanical behavior are an exciting class of materials with significant application potential in self-deployable structures, biomedical implants, and small scale actuators. A few examples include: thermally activated swelling of hydrogels (Qiu and Park, 2001; Westbrook and Qi, 2008); thermally induced scissioning and healing of elastomers (Rottach et al., 2007; Wineman and Shaw, 2007); thermally-stimulated shape memory in polymers (Behl and Lendlein, 2007; Qi et al., 2008); thermally and photo-activated bending of liquid crystal elastomers (Dunn, 2007; Hon et al., 2008; Warner and Terentjev, 2003a); and photo-activated elastomers (Jiang et al., 2006; Lendlein et al., 2005; Scott et al., 2005).

Although the underlying mechanisms coupling environmental stimulation and mechanics differ fundamentally among the material systems mentioned above, they all involve an evolution of the material structure which ultimately results in a mechanical response. For several materials, the environmental stimulus elicits a phase transformation with different phases exhibiting markedly different mechanical properties such as photo induced isotropic to nematic transition in liquid crystal elastomers (Warner and Terentjev, 2003b). However, in other material systems, environmentally stimulated evolution relaxes the state of stress and thus effectively changes the stress-free configuration of the material. This latter phenomenon is found in cross-linked networks which undergo rearrangement in response to a temperature change (Rottach et al., 2007; Wineman and Min, 2003) or light (Long et al., 2009; Scott et al., 2005). For these materials, environmentally stimulated relaxation may be modeled as a collection of parallel networks, or phases, with differing stress-free configurations.

---

[*] Email: *qih@colorado.edu*

This work focuses on the photomechanics of a recently developed light-sensitive network polymer (Scott et al., 2006; Scott et al., 2005). In a photomechanical actuation cycle in these previous studies, this material was deformed to a specified shape, and then, while the deformation was held, the material was irradiated with a light of a particular wavelength, which caused the stress to relax in the material. Under *optically thin* conditions, the intensity and associated photo-induced stress-relaxation are nearly uniform throughout the material. After the irradiation treatment and upon subsequent release of the mechanical constraints, the material remains in the specified deformed shape. However, under *optically thick* conditions, the intensity is strongly attenuated along the light path, and consequently, the corresponding stress-relaxation varies significantly along the light path. After the irradiation treatment, the material deforms to a new shape upon release of the external constraints due to the spatial variation of the internal stresses. Optically thin and thick conditions are discussed in a previous work (Long et al., 2009). The underlying molecular mechanism for photo-induced stress relaxation operates as follows: deformation of the material lowers the conformational entropy of the network by partially aligning polymer chains. Then, light triggers photo-chemical reactions that release free-radical molecules. These free radicals cleave and reform the polymer chains, which restores the network to a higher state of conformational entropy thus relieving the macroscopic state of stress. As the photo-chemical reaction continues and the network is rearranged, the macroscopic stress is further diminished. A more detailed description of molecular mechanism can be found in the work by Scott et al. (Scott et al., 2005) and Long et al. (Long et al., 2009)

From the viewpoint of continuum mechanics, a material point is assumed to contain numerous polymer chains. Deformation of the material point causes all of its associated chains to stretch. As the material is irradiated, a subset of these chains undergoes the radical-mediated cleavage, reformation, and rearrangement process such that the stress in this collection of chains is eliminated in the current configuration of the material point. Now, upon further deformation of the material point, the mechanical response of this small collection of chains is different from the remaining set of chains. Therefore, this small collection of rearranged chains and the set of remaining, unaltered chains can be regarded as different "phases" in the material, distinguished by their respective volume fractions, stress-free configurations, and deformation states. As the irradiation and radical activity continue, more chains undergo stress-relaxation and form new phases.

A central challenge in modeling the mechanics of materials with evolving phases is addressing the coupling between phase evolution and mechanical behavior. Specifically, phases formed at different times and in different configurations have different stress-free configurations and deformation states. Tracking deformations in these phases becomes computationally expensive as the number of phases with distinct deformation states increases with time. This subtlety has largely been ignored in previous theoretical work by considering special environmentally-stimulated mechanical scenarios where phase evolution occurs nearly in a single configuration. For example, in amorphous SMPs, the transition from the rubbery phase to the glassy phase typically occurs under a fixed state of deformation (Liu et al., 2006; Qi et al., 2008). Also, in the modeling of thermally and photo-induced network rearrangement, previous work has only considered material evolution in a single configuration (Long et al., 2009; Wineman and Shaw, 2007). However, environmentally stimulated actuation may require simultaneous phase evolution and material deformation. As discussed above, the deformation states are different for the phases formed at different times. Therefore robust models must include capabilities to track the deformation kinematics and evolution behaviors of individual phases.

In this paper, we model the photomechanics of light-activated, network rearranging polymers subjected to simultaneous deformation and network evolution. We then apply the model to the case of photo-induced creep behavior where a constant force is applied to the material during light irradiation. Note that photo-induced creep behavior yields a strong coupling between phase evolution and deformation as the material deforms continuously during light irradiation. This paper is organized in the following manner. Section 2 develops the theoretical framework to model the photomechanics of this material. This framework involves models for: light propagation; photochemistry; radical-mediated network (or phase) evolution; and the constitutive behaviors of each phase. Section 3 describes materials and experiments. Section 4 explores the photo-induced creep behavior of this material under a variety of photo and mechanical conditions through model predictions and experimental results.

2. Theory

To model the photomechanics of this system, it is helpful to consider a physical picture of the material during photo-activated stress relaxation and creep experiments. First the material is deformed from its original (reference) configuration to an intermediate configuration, which results in partial chain alignment and a decrease in network conformational entropy. With the deformation or external force held, the material is then irradiated at a specified wavelength. Light passing through the material triggers photochemical reactions that generate free radical molecules. These free radicals break and reform the chains allowing the network to return towards a state of higher conformational entropy, which results in macroscopic stress relaxation. From the perspective of continuum mechanics, the stress-free configuration of the material changes as a result of the network cleavage, reformation, and rearrangement. Stress relaxation and creep differ from this point forward. In stress relaxation, the intermediate configuration is fixed, so that the stress-free configuration of the material approaches that of the fixed configuration. However in creep, as the network relaxes, the material must stretch further to maintain the nominal stress, and thus, the intermediate configuration continuously changes. Modeling the changing intermediate configuration provides a significant challenge and is discussed at length in section 2.3.

We model the photomechanics of this system following the similar approach developed in our previous work (Long et al., 2009). From that analysis, four sets of sequentially-coupled physical phenomena must be addressed including: light propagation, photochemistry, radical-induced network (phase) evolution, and the solid mechanics. The first three are briefly presented in sections 2.1 and 2.2. For a more comprehensive discussion, the reader is directed towards previous work (Long et al., 2009). This paper focuses on the mechanics of network rearrangement, which is discussed in detail in sections 2.3 and 2.4. Section 2.5 describes numerical implementation of the model.

2.1. Light Propagation

We assume that the material is structurally and chemically homogenous and thus without internal boundaries. In addition, we assume that the material is irradiated with monochromatic light, consistent with the companion experiments. Light propagation through a homogenous medium without internal sources or scattering is described by the Radiative-Transfer equation (Davis and Marshak, 2004):

$$\mathbf{\Omega}(\mathbf{y},t) \bullet \nabla I(\mathbf{y},\mathbf{\Omega},t) = -\sigma(\mathbf{y},t) I(\mathbf{y},\mathbf{\Omega},t). \tag{1}$$

Here, $\mathbf{\Omega}$ and σ are the light direction and extinction fields respectively, which depend on the time, t, and position, $\mathbf{y}$, of the body in the intermediate configuration during irradiation. Because the body is initially deformed prior to irradiation, the position, $\mathbf{y}$, is different from the body's reference position, $\mathbf{x}$. Depending on the mechanical boundary conditions, the intermediate position, $\mathbf{y}$, may also be a function of time. The direction field represents the direction of propagation of the intensity field, and is uniform in space and constant during irradiation for all experiments and modeling performed in this work. The extinction field, $\sigma(\mathbf{y},t)$, determines the spatial depletion rate of the intensity field and is directly connected to the photochemistry.

2.2 Photochemistry

Light propagation through the material induces a sequence of photochemical events. First, photons are absorbed by embedded photoinitiator molecules which then chemically disassociate into free radical molecules. Second, free radicals bind to the polymer backbone and reactively move along it by cleaving and reforming it; this process results in the evolution of the network. The production of free radicals is modeled as,

$$\frac{\partial C_R(\mathbf{y},t)}{\partial t} = m \frac{\left[\alpha_i \varphi_i C_i(\mathbf{y},t) I(\mathbf{y},t)\right]}{N_A h \nu} - k_{Term}\left(C_R(\mathbf{y},t)\right)^n. \tag{2}$$

Here, C_R and C_I are the concentration fields of free radicals and initiators; N_A, h, and ν represent Avogadro's number, Planck's constant, and the monochromatic frequency of light chosen specifically for to react with the photo initiator. The first term on the right-hand side of Eq. (2) describes the rate of production of free radicals from photon-initiator reactions. For each photon-initiator reaction, m free radical molecules are generated, where m is an integer. Here, m is two (Goodner and Bowman, 2002). Not all photons absorbed by initiator molecules lead to photo-initiation events, but rather, a quantum efficiency, φ_i, is associated with this process and is here assumed to be one-half (Faria

and Steenken, 1997). The constant, α_i, represents the molar absorptivity of the initiators. Radicals do not typically exist indefinitely. Rather, termination occurs when radicals encounter, recombine and annihilate each other. Two constants characterize the rate of termination, k_{term} and *n*. The first constant is difficult to determine experimentally and is instead estimated to set the radical concentration to an appropriate magnitude based on the literature (Odian, 2004). The termination exponent, *n*, defines how many radical molecules are involved per termination event. *n* can be estimated based on related material systems, and is found to be unity (Cook et al., 2008; Scott et al., 2006).

Photon-initiator reactions consume the embedded initiator molecules, and only occur with photons with particular frequencies. We model the time evolution of the initiator concentration field as a first order photochemical equation (Terrones and Pearlstein, 2001):

$$\frac{\partial C_i(\mathbf{y},t)}{\partial t} = -\frac{\left[\alpha_i \varphi_i C_i(\mathbf{y},t) I(\mathbf{y},t) \right]}{N_A h \upsilon}. \tag{3}$$

The first term on the right-hand side of Eq. (3) differs from the corresponding term in Eq. (2) by a factor of –*m*, which indicates that the photoinitiator consumption is concomitant with the production of *m* free radicals. Eq. (3) is a standard photo-initiation modeling approach in the literature (Odian, 2004; Terrones and Pearlstein, 2001). For optically thin samples, initiator and radical concentration fields are nearly uniform across the material for all experiments so that diffusion is insignificant and neglected in this analysis.

Photoinitiators, free radicals, and the polymer matrix can all absorb photons and hence attenuate light, and their combined absorbance defines the extinction field as

$$\sigma(\mathbf{y},t) = \alpha_i C_i(\mathbf{y},t) + \alpha_R C_R(\mathbf{y},t) + A_{matrix}, \tag{4}$$

where α_i and α_R are the molar absorptivities of photoinitiators and free radicals. A_{matrix} is the absorbance of the network. Eq. (4) assumes that any products generated through photoinitiation reactions, other than radicals, do not absorb light. This assumption can easily be removed by adding additional terms to Eq. (4) that account for absorption due to other molecular species.

2.3 Radical Mediated Network Rearrangement

From a continuum mechanics viewpoint, radical-mediated network rearrangement relaxes stress by changing the stress-free configuration of the material. Based on this picture, we phenomenologically model the stress-relaxation effect of radical-mediated network rearrangement through the decomposition of the cross-linked network into multiple parallel networks, or phases, that locally account for the photo-chemical history and associated changes to the stress-free configuration of the material.

In the current study, phase formation is a time-dependent continuous process. During a small time increment of light irradiation, a small volume fraction new phase formed. The underlying network reformation mechanism suggests that the stress-free configuration of each phase should be chosen as the configuration during which the phase is formed. Phases formed at different times are therefore distinguished by their volume fractions, stress-free configurations, and deformation states. This imposes a great computational challenge in tracking the deformation state of phases formed at different times, which is discussed in detail in previous work (Long et al., 2010). To overcome this difficulty, we model the material using three phases: an *initial phase*, which is stress-free in the reference configuration of the body, a *reformed phase*, which is stress-free in an intermediate configuration based on the photo-history, and a *newly formed phase*, which is stress-free in the current configuration of the material point. At a particular time while radical-mediated network rearrangement is occurring, the evolution of each phase is modeled in two steps. First, the newly formed phase is generated from the initial and reformed phases, and the mechanical behaviors all three phases are determined. Then, the newly formed phase is reincorporated into the reformed phase by combining their volume fractions and averaging their distinct stress-free configurations. A schematic of these two steps is shown in Figure 1 for the case of creep.

In Figure 1, in order to illustrate a creep condition, a weight of W is hung under the sample. At time *t* (Figure 1a), the material is shown with two phases: initial phase (I.P.) and reformed phase (R.P.). These two phases have different deformations: I.P. has a stretch ratio of λ_t which is calculated using the initial configuration as reference configuration; R.P. is an effective phase and has a stretch ratio of $\bar{\lambda}_t$ with its reference configuration determined by the photo-mechanical history of the material. In general, $\bar{\lambda}_t \neq \lambda_t$. Figure 1b-d shows the anatomy of mechanics at time $t+\Delta t$. First, at time $t+\Delta t$, a small volume fraction of new phases (N.P.) is formed (Fig 1b). As discussed above, the new phase has no deformation at the moment of its creation, which disrupts the force balance. Therefore, the material,
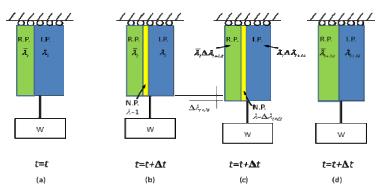
Figure 1. Schematic of simultaneous creep deformation and phase evolution. The blue, green, and yellow regions represent the initial (I.P.), reformed (R.P.), and newly (N.P.) created phases, respectively. (a) at time t, the material consists of two phases: I.P. with a stretch ratio of λ_t and R.P. with a stretch ratio of $\overline{\lambda}_t$. (b) at time $t + \Delta t$, a small volume fraction of N.P. forms; this N.P. is unstretched at the moment of creation. (c) In order to balance the external load (W), all the three phases are stretched $\Delta\lambda_{t+\Delta t}$ by. (d) R.P. is updated with a new effective stretch $\overline{\lambda}_{t+\Delta t}$, and the material point is represented by two phases at the end of $t + \Delta t$.

including all the three phases, is then stretched by $\Delta\lambda_{t+\Delta t}$ (Figure 1c). The stretch ratios in the three phases become: $\lambda_t \Delta\lambda_{t+\Delta t}$ for I.P., $\overline{\lambda}_t \Delta\lambda_{t+\Delta t}$ for R.P., and $\Delta\lambda_{t+\Delta t}$ for N.P. Finally, the N.P. is incorporated into the R.P. and the stretch ratio in the R.P. is updated to a stretch ratio of $\overline{\lambda}_{t+\Delta t}$. A detailed description of the model follows.

We model the time evolution of the volume fractions of the initial and reformed phases with the following rule,

$$\frac{df_i(\mathbf{y},t)}{dt} = -k_1 C_R(\mathbf{y},t) f_i(\mathbf{y},t)^{k_2} . \tag{5}$$

Here, i denotes either the initial or the reformed phase. k_1 and k_2 are constants that connect the rate of phase evolution to the radical concentration and network reformation history. Direct proportionality is assumed through k_1 between C_R and the time rate of change of the ith phase volume fraction. k_2 accounts for possible network evolution history effects wherein the rate of network reformation changes as the phases evolve. If there are no network reformation history effects, then k_2 takes the value of unity, and in that specific case, Eq. (5) is similar to an evolution rule previously explored (Long et al., 2010).

Uniaxial extension experiments performed before and after the photo-induced stress relaxation tests demonstrate that the shear modulus, and therefore total cross-link density, remains unchanged from the photo-mechanical treatment (Scott et al., 2005). This observation suggests that the constitutive behavior of all phases is the same (only the stress-free state differs among them) and the total volume fraction of all phases is always unity which results in the following constraint on the volume fraction of the newly formed phase,

$$\frac{df_{newly\,formed}(\mathbf{y},t)}{dt} = -\left(\frac{df_{initial}(\mathbf{y},t)}{dt} + \frac{df_{reformed}(\mathbf{y},t)}{dt} \right). \tag{6}$$

The newly formed phase is distinct from the reformed phase because it is stress-free in the current configuration, $\mathbf{y}$, while the reformed phase is stress-free in an intermediate configuration determined via the photo-mechanical history. However, after the mechanical response of the material point has been determined, the newly formed phase is incorporated into the reformed phase, and the stress-free kinematics of the reformed phase is updated.

2.4 Constitutive Behavior of the Individual Phases

Since this material is an amorphous, chemically crosslinked polymer that is photo-mechanically activated above its glass transition temperature, it is reasonable to model it as an incompressible, hyperelastic solid. Moreover, as discussed in section 2.3, the shear modulus, and consequently the cross-link density, is invariant to the photo-history. Therefore, we assume all phases exhibit the same constitutive behavior and are mechanically distinguished only by the kinematics associated with their respective stress-free configurations.

In the experiments performed, specimens are subjected to no more than 35% nominal strain, and strain stiffening is not observed. Therefore, the neo-Hookean constitutive model is used for all phases. The Helmholtz free energy and Cauchy stress for the ith phase are

$$W_i = \frac{\mu}{2}\left(I_1(\mathbf{B}_i) - 3\right) = \frac{\mu}{2}\left(\lambda_i^2 + \frac{2}{\lambda_i} - 3\right), \tag{7}$$

$$\sigma_i = \lambda_i \frac{\partial W_i}{\partial \lambda_i} = \mu\left(\lambda_i^2 - \frac{1}{\lambda_i}\right). \tag{8}$$

Here, μ is the shear modulus, which is uniform for all phases. $I_1(\mathbf{B}_i)$ is the first invariant of the finger deformation tensor, $\mathbf{B}_i = \mathbf{F}_i \mathbf{F}_i^T$, which is a function of the deformation gradient, $\mathbf{F}_i$, that either the initial, reformed, or newly formed phase experiences relative to its stress-free configuration. Incompressibility and traction-free lateral boundary conditions have been assumed in eqs. (7-8) and (8), and the axial stretch in the ith phase is given as λ, $\bar{\lambda}$, and $\Delta\lambda$ for the initial, reformed, and newly formed phases respectively. Combined, the free energies and Cauchy stresses of all phases describe the overall behavior as

$$W(t) = \sum_i f_i(t) W_i(\lambda_i, t), \tag{9}$$

$$\sigma = \sum_i f_i(t) \sigma_i(\lambda_i, t). \tag{10}$$

Again, sums over i consider all three phases.

We now describe the axial behavior of a material point, which is sufficient to model stress-relaxation and creep behaviors. Consider the Cauchy stress, at a given time, t, after the newly formed phase has been reincorporated into the reformed phase,

$$\sigma(t) = f_{initial}(t)\sigma_1(\lambda_t) + f_{reformed}(t)\sigma_2(\bar{\lambda}_t). \tag{11}$$

Here, λ_t is the total stretch and $\bar{\lambda}_t$ is the effective stretch of the reformed phase associated with prior network evolution. Over the next time increment, Δt, suppose that the material point sustains simultaneously additional deformation and radical-mediated phase evolution, which generates a newly formed phase out of the initial and reformed phases via eqs. (5-6). By the parallel decomposition of the network and assuming that all three phases experience the same increment in deformation, $\Delta\lambda_{t+\Delta t}$, the Cauchy stress may be written as,

$$\sigma(t + \Delta t) = \left(f_{initial}(t) + \int_t^{t+\Delta t} \frac{df_{initial}}{d\tau}d\tau\right)\sigma_1(\lambda_t \Delta\lambda_{t+\Delta t}) + $$
$$\cdots \left(f_{reformed} + \int_t^{t+\Delta t} \frac{df_{reformed}}{d\tau}d\tau\right)\sigma_2(\bar{\lambda}_t \Delta\lambda_{t+\Delta t}) + f_{newly\,formed}\,\sigma_2(\Delta\lambda_{t+\Delta t}) \tag{12}$$

where $f_{newly\,formed} = -\int_t^{t+\Delta t}\left(\frac{df_{initial}}{d\tau} + \frac{df_{reformed}}{d\tau}\right)d\tau$ is given by eq. (6). Eq. (12) can be used either to compute the current Cauchy stress or to determine, iteratively for example, the total stretch increment, $\Delta\lambda_{t+\Delta t}$. Then, returning to Eq. (11) with information from Eq. (12) at the current time, the effective stretch in the reformed phase, $\bar{\lambda}_{t+\Delta t}$ can be determined. An extensive discussion on this procedure has been performed in previous work (Long et al., 2010).

2.5 Implementation

Radiative transport, eq. (1), and the coupled photochemistry, eqs. (2-4), are solved in one-dimension using the finite element method (COMSOL MULTIPHYSICS) with 30 linear elements through the sample thickness, which was verified to be sufficient for convergence of the intensity, radical concentration, and initiator concentration. The radical concentration, which shows relative spatial variations of less than 10% at all times for the photochemical conditions of these experiments, is approximated to be uniform through the material. This concentration vs. time is then

passed into a MATLAB code which calculates the network evolution and mechanical response of a single, material point. As is shown and discussed in the results section, both photo-induced stress relaxation and creep experiments indicate that up to the nominal strains considered, nearly 35% in the largest creep case, the rate of network evolution is not affected by applied stretch. This result was found in a previous investigation for stress relaxation alone (Long et al., 2009). Consequently, a one-way coupling is assumed between the network evolution and the mechanical behavior. The algorithm and detailed equations for solving the one-way coupled phase evolution and mechanical response can be found in previous work (Long et al., 2010).

3. Materials and Methods

Sample preparation follows the previous work by Bowman and coworkers (Scott et al., 2005; 2006; Cook et al., 2008). Here we only briefly describe the relevant details. Resin consisting of 50 wt% of pentaerythritol tetra(3-mercaptopropionate) (PETMP) and 50 wt% 2-methylene-propane-1,3-di(thioethylvinylether) (MDTVE) was formulated with two photoinitiators, 1.0 wt% Irgacure 819 and 3.0 wt% Irgacure 184. Irradiation of the uncured, formulated resin with visible light at 40 mW cm^{-2}, 400-500 nm, consumes Irgacure 819, generating radicals and initiating the polymerization. Irgacure 184 does not absorb visible light and thus is not consumed during the polymerization. Consequently, it is available for the generation of radicals in cured specimens upon ultraviolet irradiation (365 nm). For all irradiations, the UV light source (Acticure 4000) with various interference filters was used, and intensities were measured using a radiometer (International Light IL1400A). Specimens were photopolymerized into films 190.5 μm in thickness, and were measured to be optically thin with a light path travelling through this thickness. Here, the intensity was measured at a fixed distance from the source before and after the specimens were placed in between the source and the radiometer; the intensity was attenuated by less than 10%. The rubbery Young's modulus at room temperature was determined to be 10.33 MPa via uniaxial extension measurements on an MTS Insight 2 testing system with a 5 N full capacity load cell. This Young's modulus of 10.33MPa is equivalent to 3.44MPa shear modulus under the incompressible assumption. The mechanical set-up was used for all photo-induced stress relaxation and creep experiments.

Two types of photomechanical experiments, photo-induced stress relaxation and creep, were performed on flat strips (approximately 20 mm (L) × 8 mm (W) × 0.191 mm (T)). The photo-induced stress relaxation protocol consisted of subjecting specimens to an applied nominal strain, and then, while holding this strain, specimens were irradiated with UV (365 nm) light at a specified intensity. The nominal stress necessary to maintain the applied strain was measured during irradiation. The applied nominal strain and the intensity of light were parameters that were varied from test to test. After 1 hour of irradiation, the light was turned off. The photo-induced creep protocol proceeded similarly. First, specimens were loaded to a target nominal stress, which was maintained for the remainder of the test. One minute after reaching the target nominal stress, the specimens were irradiated at a specified intensity with UV light. After one hour of irradiation, the light was turned off, and the specimen's length was recorded for another 15 minutes. Throughout the test, the specimen's length, was measured using a laser extensometer (EIR LE-05).

4. Result

In this section, we discuss model fitting and predictions of stress relaxation and creep responses, respectively. In all experiments in this work, irradiation occurs nearly uniformly and normal to the exposed region. Moreover, based on the photochemical constants, intensities, and specimen thickness, the intensity, initiator, and radical concentration fields are nearly uniform through the sample thickness. The rubbery shear modulus of the material was measured before and after irradiation treatments. For all specimens tested, no significant change was observed in the modulus as a result of irradiation treatment, and therefore, it is assumed that each network behaves with the same initial shear modulus.

The model has 11 material parameters (Table 1). Among these parameters, 8 are associated with radiative transfer and photochemistry and were therefore determined from the literature or chemical data sheets. With these parameters, we first present the average radical concentration fields through the specimen thickness vs. time under 40, 20, and 4 mW cm^{-2} intensities at 365 nm. One additional material parameter, which is material's shear modulus, can be determined from the initial slope of stress-strain curve. We then use a representative photo-induced stress relaxation experiment to determine two parameters in the network evolution laws, eqs. (5-6), and present the resultant network evolution behavior at the three different intensities previously mentioned. All model parameters are listed in Table 1. With these parameters known, we predict the photo-induced stress creep behavior at both different intensities and under different applied nominal stresses. In all cases, model predictions are compared with experiments.

The average radical concentration data through the sample thickness is presented against time for specimens exposed to 40, 20, and 4 mW cm^{-2} in Figure 2. Increasing the intensity results in a larger, initial radical concentration as well as a larger variation in the radical concentration over the time period considered. Since, according to eq. (5), the radical concentration affects the rate of network reformation directly, Figure 2 indicates how one should choose the intensity for a particular application. Specifically, if a rapid stress relaxation response is needed, then a large intensity must be used when all other experimental conditions are fixed.

Table 1. Model Parameters. The following constants were determined from these references: α_I and C_{I0} (CIBA, 2001); φ_I (Faria and Steenken, 1997); m (Goodner and Bowman, 2002); n (Cook et al., 2008).

Description	Parameter	Value
Radiative Transfer and Photochemistry		
Incident Intensity	I_0 (mW cm^2)	40, 20, 4
Photoinitiator molar absorptivity	α_I (L mol^{-1} cm^{-1})	15.94
Radical molar absorptivity	α_R (L mol^{-1} cm^{-1})	0
Initial photoinitiator concentration field	C_{I0} (mol L^{-1})	0.142
Radical termination Constant	k_{term} (L mol^{-1})$^{n-1}$ s$^-$	1.0e3
Number of radicals developed per photoinitiation event	m ()	2
Radical termination exponent	n ()	1
Quantum efficiency of photoinitiation	φ_I ()	0.5
Irradiation Wavelength	λ (nm)	365
Mechanical Properties		
Rubbery Shear Modulus	μ (MPa)	3.4
Network Evolution Rule Parameters		
Radical Concentration Proportionality Constant	k_1 (L mol^{-1} s^{-1})	45
Network Evolution Exponent	k_2 ()	3.6

The network evolution parameters, k_1 and k_2, associated with eqs. (5-6) were used to fit to the model to a representative 6% nominal strain, stress relaxation experiment irradiated at 40 mW cm^{-2} using the radical concentration in Figure 2; the simulation and experimental results are shown in Figure 3 where both curves are normalized to their respective stresses immediately before irradiation. Overall, the model fit the experimental data very well. From Figure 3, initially, the model fit slightly exceeds the experiment with regards to the rate of stress relaxation. By 100 seconds, both curves exhibit a shift to a slower rate of stress relaxation, and this shift appears more suddenly in the experiment than in the model. Consequently, by 1000 seconds, the model has again slightly over predicted the stress relaxation response, but by two and three thousand seconds, the model and experiment agree well.

With the parameters, k_1 and k_2, determined by fitting the model to the experiment in Figure 3, the radical mediated network evolution is presented in Figure 4, which shows the reformed phase volume fraction vs. time for each of the corresponding radical concentration curves in Figure 2 as computed through eqs. (5-6). At 40mW cm^{-2} irradiation, the reformed phase is initially generated quickly such that nearly half of the network has been reformed after five minutes. However, between five and ten minutes, there is a sharp transition so that further network reformation is comparatively slow with only an addition quarter of the volume fraction reforming in the remaining 55 minutes.

This transition is controlled by the network evolution parameter, $k_2 = 3.6$, in eq. (5). When k_2 is larger than unity, phases with larger volume fractions evolve faster than phases with smaller volume fractions. Consequently in this material, the initial phase evolves quickly early on, but as the initial phase declines, its continued rate of evolution and hence transformation into the newly formed and then reformed phases decreases rapidly. Therefore, the volume fraction of the reformed phase no longer increases significantly. When irradiated at 20 mW cm^{-2} the behavior is similar to the 40 mW cm^{-2} cases with an initial, rapid response, followed by significantly slower phase reformation after a discernable transition. The difference between the 20 and 40 mW cm^{-2} cases is that initially, the rate of reformation is slightly slower for the 20 mW cm^{-2} irradiation, and, at later times, the rate of reformation is slightly faster. In contrast to the previous two cases, the 4 mW cm^{-2} irradiation phase evolution behavior does not show a strong transition. Instead, the initially fast rate of reformation broadly transitions to a slower rate, but the transition extends broadly between ten and thirty minutes. Recall that this model assumes that the state of deformation in the material does not affect the rate of
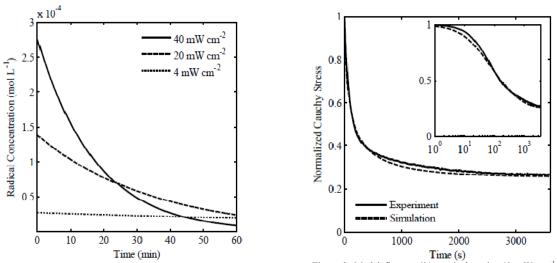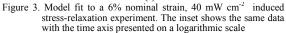
Figure 2. Average concentration through the sample thickness as a function of time for three different intensities at 365nm.

Figure 3. Model fit to a 6% nominal strain, 40 mW cm⁻² induced stress-relaxation experiment. The inset shows the same data with the time axis presented on a logarithmic scale

network reformation, and therefore, the network evolution responses presented here apply both to the stress relaxation curves in Figure 3 as well as to all subsequent simulations.

The model's prediction capabilities are now validated against photo-induced creep experiments under a variety of intensity and applied nominal-stress conditions. Note that these experiments provide an additional complexity of changing configurations that is not present in the stress relaxation experiment used to fit the model. First, three creep predictions are made for specimens under an applied nominal stress of 500 kPa and irradiated at 40, 20, and 4 mW cm⁻² respectively. Model predictions and corresponding experiments are given in Figure 5.
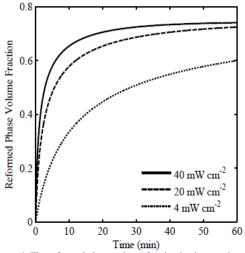

Figure 4. The reformed phase volume fraction is given against time corresponding to both the intensities reported and the associated radical concentration profiles in Figure 2
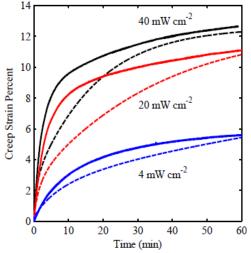

Figure 5. Photo-induced, nominal creep strain percents from model predictions (dashed lines) and corresponding experiments (solid lines) for specimens subjected to 500 kPa nominal stress and intensities of 40 (black), 20 (red), and 4 (blue) mW cm⁻².

The model reasonably predicts the overall experimental creep results in all three cases. The experimental creep curves exhibit three distinct regions in chronological order: an initial region characterized by a rapid creep response; an intermediate region wherein the rate of creep slows; and a steady region when the rate of creep is nearly constant. The initial, 0-5 minutes, and steady, 40-60 minutes, regions of the model and experiment are similar for all three intensities, but at intermediate times, 5-40 minutes, the model under-predicts photo-induced creep.

Two salient features of the model curves differ from their corresponding experiments. First, the model curves exhibit a broader creep rate transition in the intermediate region than seen experimentally. This difference is particularly evident with the 20 and 40 mW cm^{-2} curves in which the experiments show very sharp transitions while transition shown in the 4 mW cm^{-2} case is adequately represented by the model. Second, the model curves slightly over predict the rate of the steady creep behavior compared with experiments. Furthermore, the model suggests that the steady creep rate decreases slightly as the intensity is increased. This behavior can be understood by considering the effects of increasing the intensity on the radical concentration profile in Figure 2 and the corresponding reformed phase evolution in Figure 4. With higher intensity, the radical concentration profile undergoes a greater variation over the irradiation period such that the rate of reformed phase evolution, and hence the creep rate, is slower at later times than when the radical concentration is more uniform in time (at lower intensities). However, experimentally, the steady creep rate increases slightly with heightened intensities. One possible explanation for this behavior is that the MDTVE functionalities (constituents of the polymer chains), which are cleaved and reformed by the radicals, also are cleaved and reformed directly from 365 nm light but at a slower rate than that produced by the action of the radicals. A control creep experiment was performed to probe this hypothesis in which a specimen without residual initiator (0 wt% instead of 3 wt% Irgacure 184 initiator) was subjected to creep at 500 kPa nominal stress. In this experiment, the specimen sustained 2% nominal creep strain after one hour of irradiation at and 40 mW cm^{-2} intensity. However, because this final creep strain was only half of the creep strain seen in the steady creep region of the similar experiment in Figure 5, this additional stress-relaxation mechanism was not included in the model.

Next, the model is used to predict photo-induced creep at a fixed intensity of 40 mw cm-2 and applied nominal stresses of 100, 500 and 1000 kpa respectively as shown in Figure 6a-b. Although multiple specimens were tested for the 1000 kpa trial, they consistently broke near 25 % creep strain (~35% strain overall), but the model is used to predict the behavior as if these specimens would survive for the full hour of irradiation.

The model predicts the overall creep behavior of each applied nominal stress. Again, the three experiments exhibit three regions of behavior: large creep rates initially; a slowing of the rate of creep at intermediate times; and a steady creep rate late in the experiments. As with the intensity-creep study, the model does not predict such a creep rate transition and under predicts the initial creep rate. Consequently, the model and experiment differ significantly in the vicinity of the transition, between 5-20 minutes. Later, results agree between the experiment and creep at 100 and 500 kPa.

Figure 6b, which shows all six creep curves normalized to their nominal creep strains at twenty minutes, collapses both the model and experimental data onto two master curves. Note that noise in the 100 kPa curve is amplified through this normalization, but its trend is clear. Figure 6b, which shows all six creep curves normalized to their nominal creep strains at twenty minutes, collapses both the model and experimental data onto two master curves. Note that noise in the 100 kPa curve is amplified through this normalization, but its trend is clear. This result is expected for the model because it has been implemented under the assumption that the state of deformation in the material does not influence the rate of network evolution. Because it is also observed in the experimental master curve, we conclude that network evolution for this material system is not influenced by the state of deformation to moderate strains. This conclusion was also found in photo-induced stress relaxation experiments stretched to different nominal strains in previous work (Long et al., 2009). Only a slight spread of the master curve is observed in the model at later times which arises from the difference in mechanical boundary conditions. This observation cannot be made accurately with the experiments because 1000 kPa curves could not be crept successfully for one hour, but the 100 and 500 kPa curves show similar steady creep behavior at later times without significant spreading.

The salient feature of both the stress relaxation and creep experiments presented in this work is that a sharp transition occurs between the initial, rapid response of the material and the slower response at later times. Capturing this transition is the key to modeling the overall photo-mechanical behavior, but interestingly, such a sharp transition is not observed in the underlying, simulated, radical concentrations shown in Figure 2, and therefore we have handled this behavior phenomenological through network evolution rules in Eq. (5-6) based on the idea that the rate of network evolution may entail history effects. This phenomenological approach is successful in modeling stress relaxation as seen here Figure 3, but it does not predict the sharp response transitions well in creep. Nevertheless, the model accurately predicts the appropriate trends associated with large changes in applied intensity and loading conditions even though neither of which are incorporated into the fitting and/or network evolution rules of eqs. (5-6).
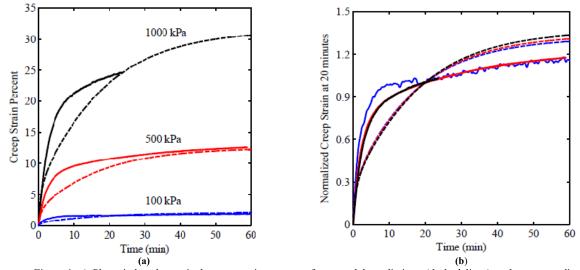
Figure 6. a) Photo-induced, nominal creep strain percents from model predictions (dashed lines) and corresponding experiments (solid lines) specimens subjected to 100, 500, and 1000 kPa nominal stresses and an intensity of 40 mW cm^{-2}. b) 100 (blue), 500 (red), and 1000 kPa (black) creep curves normalized by their respective values at 20 minutes.

Conclusions

We have explored, both experimentally and theoretically, the photo-induced creep behavior of a stress-relaxing, light-activated network polymer. Previous work on this material focused on photo-induced stress relaxation (Long et al., 2009), wherein material evolution occurs in a single (fixed) configuration. Our principal objective for this paper is to investigate simultaneous light-stimulated material evolution and deformation. In contrast to stress relaxation, photo-induced creep involves additional complexity because the material deforms continuously as the phases evolve. Here, light-stimulated activity is described through a phenomenological model that decomposes the cross-linked network into three parallel networks: an initial, reformed, and newly created network, each with an associated volume fraction and stress-free configuration. The volume fractions, stress-free configurations and deformation states of each network evolve in response to irradiation and concomitant photochemistry. The combined mechanical behaviors of all three networks represent the mechanical response of the material. Although the model has 11 material parameters, it contains only two fitting parameters that are associated with the evolution of the networks, and these are fit to a single, stress relaxation experiment. The model is then used to predict photo-induced creep behavior under different applied nominal stresses and light intensities. Generally, the model performs well in predicting the overall creep behavior of individual tests as well as capturing the trends produced by changing the light intensity and applied nominal stress. These creep tests are characterized by three behavior regions: a rapid, initial creep response followed; an intermediate response characterized by a slowing of the creep rate; and a steady creep rate at later irradiation times. The main deficiency of the model is that it does not capture the sharpness of creep rate transition in the intermediate time region, particularly at large stresses and intensities. Continued investigation is underway to predict this behavior.

Acknowledgements

References

Behl, M. and Lendlein, A., 2007. Shape-memory polymers. Materials Today, **10**(4): 20.

CIBA, 2001. Ciba® IRGACURE® **184**. 1-2.

Cook, W.D. et al., 2008. Photopolymerization kinetics, photorheology and photoplasticity of thiol-ene-allylic sulfide networks. Polymer International, **57**(3): 469.

Davis, A.B. and Marshak, A., 2004. Photon propagation in heterogeneous optical media with spatial correlations: enhanced mean-free-paths and wider-than-exponential free-path distributions. Journal of Quantitative Spectroscopy and Radiative Transfer, **84**(1): 3.

Dunn, M.L., 2007. Photomechanics of mono - and polydomain liquid crystal elastomer films. Journal Of Applied Physics, **102**(1): 013506.

Faria, J.L. and Steenken, S., 1997. Photoionization of alpha-alkoxybenzyl radicals to yield alpha-alkoxybenzyl cations. Photochemistry of omega,omega-dimethoxy-omega-phenylacetophenone in polar solvents at high light intensities. Journal Of The Chemical Society-Perkin Transactions **2**(6): 1153-1159.

Goodner, M.D. and Bowman, C.N., 2002. Development of a comprehensive free radical photopolymerization model incorporating heat and mass transfer effects in thick films. Chemical Engineering Science, 57(5): 887-900.

Hon, K.K., Corbett, D. and Terentjev, E.M., 2008. Thermal diffusion and bending kinetics in nematic elastomer cantilever. European Physical Journal E, 25(1): 83-89.

Jiang, H., Kelch, S. and Lendlein, A., 2006. Polymers move in response to light. Advanced Materials, **18**(11): 1471.

Lendlein, A., Hongyan, J., Junger, O. and Langer, R., 2005. Light-induced shape-memory polymers. Nature, **434**(7035): 879.

Liu, Y., Gall, K., Dunn, M.L., Greenberg, A.R. and Diani, J., 2006. Thermomechanics of shape memory polymers: Uniaxial experiments and constitutive modeling. International Journal of Plasticity, **22**(2): 279.

Long, K.N., Dunn, M.L. and Qi, H.J., 2010. Mechanics of Soft Active Materials with Phase Evolution. International Journal of Plasticity, **26** (4): 603-616.

Long, K.N., Scott, T.F., Qi, H.J., Bowman, C.N. and Dunn, M.L., 2009. Photomechanics of Light Activated Polymers. Journal Of The Mechanics And Physics Of Solids, **57** (7): 1103-1121

Odian, G., 2004. Principles of polymerization. Wiley-Interscience, Staten Island, New York, 812 pp. 207

Qi, H.J., Nguyen, T.D., Castro, F., Yakacki, C.M. and Shandas, R., 2008. Finite Deformation Thermo-Mechanical Behavior of Thermally Induced Shape Memory Polymers. Journal of Mechanics and Physics of Solids, **56**: 1730-1751.

Qiu, Y. and Park, K., 2001. Environment-sensitive hydrogels for drug delivery. Advanced Drug Delivery Rev., **53**: 321-339.

Rottach, D.R. et al., 2007. Molecular dynamics simulations of polymer networks undergoing sequential cross-linking and scission reactions. Macromolecules, **40**(1): 131-139.

Scott, T.F., Draughon, R.B. and Bowman, C.N., 2006. Actuation in crosslinked polymers via photoinduced stress relaxation. Advanced Materials, **18**(16): 2128.

Scott, T.F., Schneider, A.D., Cook, W.D. and Bowman, C.N., 2005. Chemistry: Photoinduced plasticity in cross-linked polymers. Science, **308**(5728): 1615.

Terrones, G. and Pearlstein, A.J., 2001. Effects of optical attenuation and consumption of a photobleaching initiator on local initiation rates in photopolymerizations. Macromolecules, 34(10): 3195.

Warner, M. and Terentjev, E., 2003a. Thermal and photo-actuation in nematic elastomers. Macromolecular Symposia, **200**: 81-92.

Warner, M. and Terentjev, E.M., 2003b. Liquid Crystal Elastomers. Oxford University Press, Oxford, 426 pp.

Westbrook, K.K. and Qi, H.J., 2008. Actuator Designs using Environmentally Responsive Hydrogels. Journal of Intelligent Material Systems and Structures, **19**: 597-607.

Wineman, A. and Min, J.-H., 2003. Time dependent scission and cross-linking in an elastomeric cylinder undergoing circular shear and heat conduction. International Journal of Non-Linear Mechanics, **38**(7): 969.

Wineman, A. and Shaw, J., 2007. Combined deformation- and temperature-induced scission in a rubber cylinder in torsion. International Journal of Non-Linear Mechanics, **42**(2): 330.